PHOTONICS Research

$CsPbBr_3$ perovskite quantum dots: saturable absorption properties and passively *Q*-switched visible lasers

Jingzhou Li,[1,2] Hongxing Dong,[1,5] Bin Xu,[3] Saifeng Zhang,[1] Zhiping Cai,[3] Jun Wang,[1] and Long Zhang[1,4,*]

[1]Key Laboratory of Materials for High-Power Laser, Shanghai Institute of Optics and Fine Mechanics, Chinese Academy of Science, Shanghai 201800, China
[2]University of Chinese Academy of Sciences, Beijing 100049, China
[3]Department of Electronic Engineering, Xiamen University, Xiamen 361005, China
[4]IFSA Collaborative Innovation Center, Shanghai Jiao Tong University, Shanghai 200240, China
[5]e-mail: hongxingd@siom.ac.cn
*Corresponding author: lzhang@siom.ac.cn

Received 19 June 2017; revised 20 July 2017; accepted 24 July 2017; posted 25 July 2017 (Doc. ID 298302); published 6 September 2017

This work presents the saturable absorption (SA) properties of $CsPbBr_3$ perovskite quantum dots (QDs). The perovskite QDs show excellent SA performance with a nonlinear absorption coefficient of -35×10^{-2} cm/GW and a figure of merit of 3.7×10^{-14} esu cm. Further, their use as saturable absorbers in a passively *Q*-switched visible solid-state laser for the generation of soliton pulses is demonstrated. These results demonstrate the potential for the perovskite QDs to act as saturable absorbers.

OCIS codes: (190.4400) Nonlinear optics, materials; (160.4670) Optical materials; (160.4760) Optical properties.

https://doi.org/10.1364/PRJ.5.000457

1. INTRODUCTION

Materials crystallizing with a perovskite structure (a ternary compound of the form AMX_3) have received considerable attention owing to their excellent ferroelectric, paraelectric, and optoelectronic properties [1,2]. Studies on these materials have been ongoing since the beginning of the last century, but have mainly concentrated upon the structural and electromagnetic properties of the compounds. Recently, lead halide perovskite semiconductors (where A = CH_3NH_3, Cs, etc.; M = Pb, Ge; X = Cl, Br, I) have returned to the focus of researchers because of their remarkable performance in photo-electronic fields [3–6]. These ternary compounds not only possess low densities for mid-gap trap states and excellent band-gap tunability, but also exhibit high photoluminescence (PL) efficiency (>90%) and narrow PL bandwidths (12–40 nm). Among them, all-inorganic $CsPbX_3$ perovskite quantum dots (QDs) have shown the potential for application in next-generation optoelectronic materials [7–9].

To date, most research on perovskite QDs has concentrated on the linear optical region. Studies on the nonlinear properties have been relatively rare, and few have focused on two-photon or multiphoton absorption and emission [10–12]. In fact, their unique quantized discrete energy structure and direct band gap imply lower saturation intensity compared to that of traditional saturable absorption (SA) materials such GaAs and two-dimensional nanomaterials (MoS_2 and graphene). Further, compared to metal chalcogenide QDs, perovskite QDs exhibit faster carrier dynamics [13]. Perovskite semiconductors also have a relatively low defect concentration, which reduces the scattering centers for non-radiative charge carrier recombination [14]. This is conductive to form the SA response. This means that perovskite QDs are promising candidate materials for saturable absorbers [15].

In this work, we focus on the SA properties of perovskite QDs using an open-aperture Z-scan technique. The perovskite QDs exhibit significant SA for femtosecond pulses at 515 nm, resulting in a nonlinear absorption coefficient of $\alpha_{NL} \sim -(35 \pm 8) \times 10^{-2}$ cm/GW. Based on the perovskite QDs acting as saturable absorbers, superior passive *Q*-switching behavior was observed.

2. EXPERIMENT

The $CsPbBr_3$ QDs were synthesized via a chemical solution route similar to a previously reported method [16]. First, a $Cs(OA)_2$ solution was obtained by dissolving $CsCO_3$ (2.394 mmol, 99.9%) in dried oleic acid (OA, 1.25 mL, 90%) and dried octadecene (ODE, 20 mL, 90%) at 150°C under N_2. Then, ODE (10 mL, 90%) and $PbBr_2$ (0.375 mmol,

99.999%) were loaded in a 50 mL three-neck flask and dried under vacuum for 30 min at 110°C. Dried OA (1 mL, 90%) and dried oleylamine (1 mL, 90%) were injected at 110°C under N_2. The mixture was heated to 160°C for 10 min under an N_2 flow. Subsequently, 0.8 mL of the $Cs(OA)_2$ solution was injected into the reaction system. After 5 s, the reaction mixture was cooled using an ice-water bath. The $CsPbBr_3$ QDs in crude solution were separated by centrifuging. After centrifugation, the nanocrystals were redispersed in toluene.

The PL quantum yields (QYs) of the sample reached up to 65% in comparison with that of the integrated emission of the QDs with Rhodamine 6G (QY = 95%). The size and shape of the $CsPbBr_3$ QDs were obtained by transmission electron microscopy (TEM) images (JEOL, JEM-2010). The linear optical absorption was recorded using a Shimadzu UV-2450 UV-VIS spectrophotometer with 1 nm incremental steps. The PL spectrum was recorded with a Cary Eclipse (Varian) fluorescence spectrophotometer. The PL decay dynamics of the sample were obtained using time-correlated single photon counting (TCSPC) measurements under excitation by a 90 ps pulsed laser diode at 3.2 eV (405 nm).

3. RESULTS AND DISCUSSION

As shown in Fig. 1(a), the $CsPbBr_3$ QDs exhibited good monodispersion and a nearly cubic shape. The edge length of most $CsPbBr_3$ QDs is concentrated at 7.6 ± 0.8 nm, which is comparable with the exciton Bohr diameters of the perovskite nanocrystals ($CsPbBr_3$: ~ 7 nm, $CsPbI_3$: ~ 12 nm) [16]. The high resolution-TEM image shows the highly crystalline nature of the perovskite QDs [Fig. 1(b)]. Figure 1(c) shows the structure schematic of the $CsPbBr_3$ perovskite QDs. The inorganic $PbBr_6$ octahedral cage shares corners to form a three-dimensional network, while the larger Cs-site cations sit in the 12-coordinate cubo-octahedral cavities within this network.

Figure 1(d) shows the linear absorption and PL spectra of the perovskite QDs at room temperature. Here, the band-edge absorption peak of the perovskite QDs was 516 nm (2.40 eV). The PL spectrum showed a full width at half maximum (FWHM) of about 24 nm (107 meV) and was centered at 526 nm (2.36 eV), which corresponded to a non-resonant Stokes shift of 10 nm (45 meV). The time-resolved PL decay curve of the QDs is shown in Fig. 1(e). By fitting with a single exponential function, we obtained a radiative lifetime of about 2 ns. The lifetime of the perovskite QDs was about one order of magnitude smaller than that of traditional metal chalcogenide QDs, for example, ~40 ns for CdTe, ~45 ns for CdTe/CdS, ~20 ns for CdSe, and ~35 ns for CdSe/CdS [17–19].

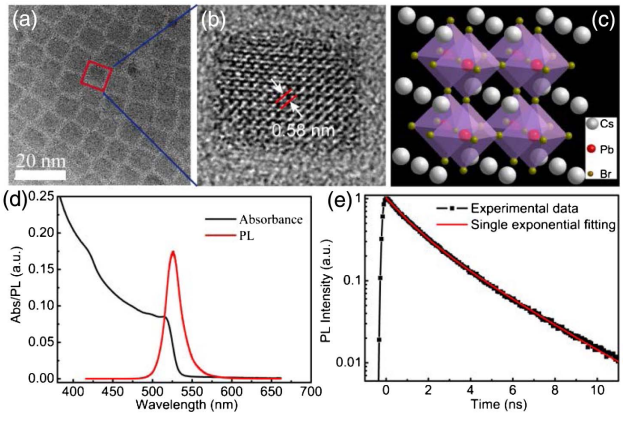

Fig. 1. (a) TEM image of the $CsPbBr_3$ perovskite QDs. (b) High-resolution TEM image of a single QD. (c) Schematic of the $CsPbBr_3$ perovskite lattice. (d) Normalized linear absorption (black) and PL (red) spectra for the $CsPbBr_3$ perovskite QD dispersion. (e) PL decay kinetics of the $CsPbBr_3$ perovskite QDs under excitation at 405 nm.

The nonlinear optical properties of the $CsPbBr_3$ QDs were studied using an open-aperture (OA) Z-scan system with a 1 kHz laser pulse and a pulsewidth of ~340 fs at 515 nm (2.41 eV). The experimental setup has been well verified in previous nonlinear optical experiments [19,20]. The linear transmittance of the perovskite QDs solution at 515 nm in a 1 mm cuvette was 93%, corresponding to the QDs concentration of $\sim 3.5 \times 10^{-9}$ mol/L. During the Z-scan measurements, we did not observe any obvious scattering signals, which indicated that the QDs maintain good stability under this excitation energy.

As shown in Fig. 2, the $CsPbBr_3$ QDs exhibited obvious SA response. The Z-scan results in Fig. 2(a) were fitted by the following nonlinear propagation equation:

$$\frac{dI_z}{dz} = -(\alpha_0 + \alpha_{NL} I_z) I_z, \tag{1}$$

where I_z represents the incident intensity at position z and α_0 and α_{NL} denote the linear and nonlinear absorption coefficients, respectively. The power transmittance $T(z)$ is obtained as shown below:

$$T(z) = \sum_{m=0}^{\infty} \frac{[-q_0(z)]^m}{(m+1)^{3/2}}, \tag{2}$$

where $q_0(z) = \alpha_{NL} \frac{I_0 L_{eff}}{1+\frac{z^2}{z_0^2}}$, $L_{eff} = \frac{1-e^{-\alpha_0 L}}{\alpha_0}$ represents the sample's effective thickness, I_0 denotes the on-axis irradiance at the focus, and z_0 is the beam's diffraction length. Here, we make m to 3, because the fitting curve does not change much whether we add the $m = 3$ term or not. The nonlinear absorption coefficient of the $CsPbBr_3$ perovskite QDs at 515 nm was about $\sim -(35 \pm 8) \times 10^{-2}$ cm/GW. The figure of merit (FOM) of the third-order optical nonlinearity is defined as FOM $= \frac{|\mathrm{Im}\chi^{(3)}|}{\alpha_0}$, which can be used to eliminate the discrepancy caused by linear absorption. $\mathrm{Im}\chi^{(3)} = \left[\frac{10^{-7} c\lambda n^2}{96\pi^2}\right] \alpha_{NL}$

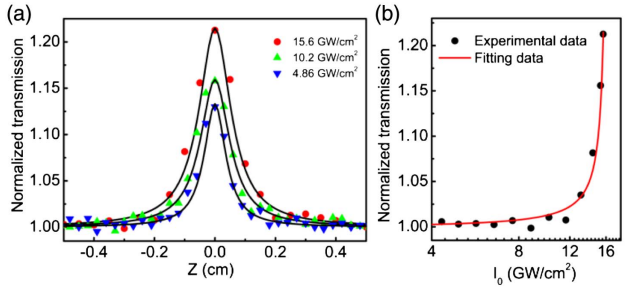

Fig. 2. (a) Open-aperture Z-scan results of $CsPbBr_3$ perovskite QDs under excitation of 515 nm, with a 1 kHz repetition rate at different intensities. (b) Normalized transmission as a function of intensity for the 15.6 GW cm^{-2} curve in (a).

Table 1. Linear and Nonlinear Optical Parameters of Different Materials

Material	λ (nm)	T (%)	α_{NL} (cm/GW, $\times 10^{-2}$)	FOM (esu cm, $\times 10^{-14}$)	I_s (GW/cm^2)	Reference
$CsPbBr_3$ QDs	515	93	−35	3.7	11	This work
CdTe/CdS QDs	515	84	−13	2.1	9	[19]
MoS_2	515	86	−1.9	0.47	72	[19,21]
Graphene	515	74	−1.2	0.15	265	[19,21]
Black phosphorous	400	71	−1.6	N/A	455	[22]
Bi_2Se_3	800	N/A	N/A	N/A	10	[23]

is the imaginary part of the third-order nonlinear susceptibility. We obtained that the FOM for the QDs was $\sim(3.7 \pm 0.85) \times 10^{-14}$ esu cm. The saturation intensity (I_s) of the QDs was obtained by the following equation:

$$\frac{dI_z}{dz} = -\left(\frac{\alpha_0}{1 + I_z/I_s} + \beta I_z\right) I_z. \quad (3)$$

The I_s of the $CsPbBr_3$ perovskite QDs could be calculated as ~11 MW/cm^2. Table 1 summarizes the linear and nonlinear optical parameters of some excellent SA materials. We found that the $CsPbBr_3$ perovskite QDs exhibited a high nonlinear absorption coefficient and FOM and a low saturation intensity. These results directly suggest that the perovskite QDs have great application potentials as saturable absorbers. It is also worth noting that the band gap of the QDs was very close to the excitation photonic energy, which meets the condition of resonance excitation. Therefore, the SA response of the QDs at 515 nm is resonant SA response. For the resonance absorption, the probability of the resonant electron transition is much larger than that of other non-resonant transitions. It can easily fill the conduction band of the QDs, and reach the saturation state. In other words, if the SA response is non-resonant optical response, the SA performance of the perovskite QD will decrease [19].

Further, based on the use of $CsPbBr_3$ perovskite QDs as saturable absorbers, the passively Q-switched visible solid-state laser was investigated. For ease of integration into the laser cavity, we needed to fabricate a polymer composite film with a $CsPbBr_3$ QD dispersion. First, a $CsPbBr_3$ perovskite QD toluene solution (with a QD concentration of $\sim 3.5 \times 10^{-9}$ mol/L) was mixed into a poly-methylmetacrylate (PMMA) toluene solution in a volume ratio of 1∶1. Then, the mixture was transferred onto thin glass substrates by a spin-coating method, followed by drying at ambient conditions. The prepared QD-PMMA film deposited on the glass substrate was used for subsequent Q-switched laser experiments. The laser setup was similar to that used in previous studies [19,24]. During Q-switched laser operation, the QD-PMMA film deposited on the glass substrate was inserted into diode-pumped $Pr:LiYF_4$ solid-state laser cavities operating at ~522 nm.

Figure 3 presents the Q-switched laser results with the $CsPbBr_3$ perovskite QDs acting as saturable absorbers. A typical oscilloscope trace with very stable pulse amplitude is seen in Fig. 3(a). In contrast, without the QDs in the laser cavities, the laser always operated at the continuous-wave regime and no pulse train was observed. Figure 3(b) shows a single laser pulse with a Gaussian-like shape, corresponding to an FWHM of ~653 ns. The laser spectrum of the Q-switching is shown

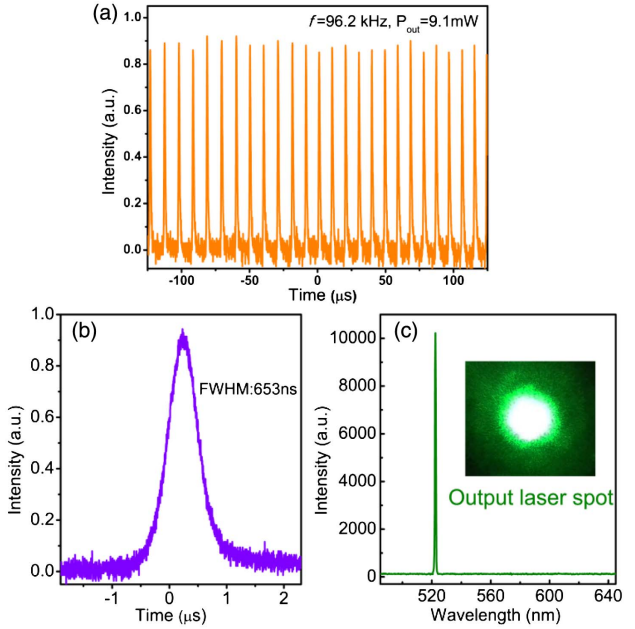

Fig. 3. Passively Q-switched laser results for the $CsPbBr_3$ perovskite QDs as saturable absorbers: (a) pulse trains measured at average output powers of 9.1 mW with a repetition rate of 96.2 kHz, (b) single pulse waveform, and (c) output laser spectrum. The inset shows the output beam spot.

in Fig. 3(c). The laser wavelength was stabilized at around 522 nm, without a significant change compared with the continuous-wave operation.

Figure 4(a) shows the variation in the average output powers against the absorbed powers. In the laser cavity with the $CsPbBr_3$ QDs, a stable pulse laser was observed when the absorbed pump power increased to 660 mW. The average output power was almost a linear function of the absorbed power. The maximum output power was up to 9.11 mW under an

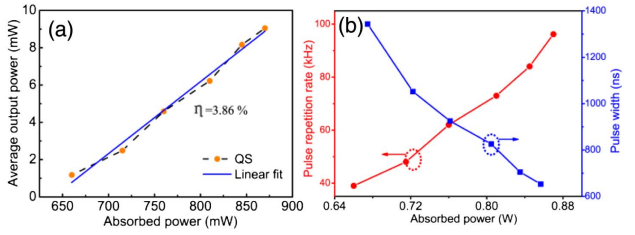

Fig. 4. (a) Laser output power characteristics of Q-switched modes. (b) Variations of pulsewidths and pulse repetition rates with increasing absorbed pump powers for the 522 nm Q-switched visible laser.

absorbed power of 870 mW, corresponding to a slope efficiency of about 3.86%. The relationship between the pulse repetition rates and pulsewidths of a Q-switched laser with absorbed pump power from 660 to 870 mW is shown in Fig. 4(b). The repetition rates could be widely tuned in the range of 36–96.2 kHz, and the pulsewidths were significantly narrowed from 1345 to 653 ns. Further, we estimated the maximum single pulse energy to be about 94 nJ. For a passively Q-switched laser operation, the pulsewidth is mainly determined by the cavity round-trip time and modulation depth of the used saturable absorber [25–27]. Therefore, by shortening the cavity length and improving the modulation depth of the QDs, the pulsewidth of the Q-switched laser can be narrowed further.

4. CONCLUSION

In summary, $CsPbBr_3$ perovskite QDs with high crystallinity were prepared using a chemical solution route. The QDs exhibited strong SA response for femtosecond pulses at 515 nm, better than the traditional SA materials. A nonlinear absorption coefficient of $\alpha_{NL} \sim -35 \times 10^{-2}$ cm/GW, an FOM of $\sim 3.7 \times 10^{-14}$ esu cm, and I_s of ~ 11 MW/cm^2 were obtained for the $CsPbBr_3$ QDs. Further, we also experimentally demonstrated passively Q-switched lasers based on the perovskite QDs acting as saturable absorbers. For a 522 nm laser, a maximum average output of 9.11 mW was achieved with a corresponding shortest pulsewidth of 653 ns and pulse repetition rate of 96.2 kHz. The results will further promote the application of perovskite semiconductor materials in nano-optics.

Funding. National Natural Science Foundation of China (NSFC) (61378074, 61475173); Youth Innovation Promotion Association Chinese Academy of Sciences (CAS).

REFERENCES

1. C. Zener, "Interaction between the D-shells in the transition metals. 2. Ferromagnetic compounds of manganese with perovskite structures," Phys. Rev. **82**, 403–405 (1951).
2. S. Jin, T. H. Tiefel, M. McCormack, R. A. Fastnacht, R. Ramesh, and L. H. Chen, "Thousandfold change in resistivity in magnetoresistive La-Ca-Mn-O films," Science **264**, 413–415 (1994).
3. W. S. Yang, J. H. Noh, N. J. Jeon, Y. C. Kim, S. Ryu, J. Seo, and S. I. Seok, "High-performance photovoltaic perovskite layers fabricated through intramolecular exchange," Science **348**, 1234–1237 (2015).
4. N. J. Jeon, J. H. Noh, W. S. Yang, Y. C. Kim, S. Ryu, J. Seo, and S. I. Seok, "High-performance photovoltaic perovskite layers fabricated through intramolecular exchange," Nature **517**, 476–480 (2015).
5. W. W. Liu, J. Xing, J. X. Zhao, X. L. Wen, K. Wang, P. X. Lu, and Q. H. Xiong, "Giant two-photon absorption and its saturation in 2D organic-inorganic perovskite," Adv. Opt. Mater. **5**, 1601045 (2017).
6. P. F. Li, Y. Chen, T. S. Yang, Z. Y. Wang, H. Lin, Y. H. Xu, L. Lei, H. R. Mu, B. N. Shivananju, Y. P. Zhang, Q. L. Zhang, A. L. Pan, S. J. Li, D. Y. Tang, B. H. Jia, H. Zhang, and Q. L. Bao, "Two-dimensional $CH_3NH_3PbI_3$ perovskite nanosheets for ultrafast pulsed fiber lasers," ACS Appl. Mater. Interfaces **9**, 12759–12765 (2017).
7. S. Yakunin, L. Protesescu, F. Krieg, M. I. Bodnarchuk, G. Nedelcu, M. Humer, G. De Luca, M. Fiebig, W. Heiss, and M. V. Kovalenko, "Low-threshold amplified spontaneous emission and lasing from colloidal nanocrystals of caesium lead halide perovskites," Nat. Commun. **6**, 8056 (2015).
8. F. Zhu, L. Men, Y. J. Guo, Q. C. Zhu, U. Bhattacharjee, P. M. Goodwin, J. W. Petrich, E. A. Smith, and J. Vela, "Shape evolution and single particle luminescence of organometal halide perovskite nanocrystals," ACS Nano **9**, 2948–2959 (2015).
9. N. Yarita, H. Tahara, T. Ihara, T. Kawawaki, R. Sato, M. Saruyama, T. Teranishi, and Y. Kanemitsu, "Dynamics of charged excitons and biexcitons in $CsPbBr_3$ perovskite nanocrystals revealed by femtosecond transient-absorption and single-dot luminescence spectroscopy," J. Phys. Chem. Lett. **8**, 1413–1418 (2017).
10. Y. Xu, Q. Chen, C. Zhang, R. Wang, H. Wu, X. Zhang, G. Xing, W. W. Yu, X. Wang, Y. Zhang, and M. Xiao, "Two-photon-pumped perovskite semiconductor nanocrystal lasers," J. Am. Chem. Soc. **138**, 3761–3768 (2016).
11. J. Z. Li, S. F. Zhang, H. X. Dong, X. Q. Yuan, X. W. Jiang, J. Wang, and L. Zhang, "Two-photon absorption and emission in $CsPb(Br/I)_3$ cesium lead halide perovskite quantum dots," CrystEngComm **18**, 7945–7949 (2016).
12. K. Wei, Z. J. Xu, R. Z. Chen, X. Zheng, X. G. Cheng, and T. Jiang, "Temperature-dependent excitonic photoluminescence excited by two-photon absorption in perovskite $CsPbBr_3$ quantum dots," Opt. Lett. **41**, 3821–3824 (2016).
13. K. F. Wu, G. J. Liang, Q. Y. Shane, Y. P. Ren, D. G. Kong, and T. Q. Lian, "Ultrafast interfacial electron and hole transfer from $CsPbBr_3$ perovskite quantum dots," J. Am. Chem. Soc. **137**, 12792–12795 (2015).
14. F. Zheng, L. Z. Tan, S. Liu, and A. M. Rappe, "Rashba spin-orbit coupling enhanced carrier lifetime in $CH_3NH_3PbI_3$," Nano Lett. **15**, 7794–7800 (2015).
15. Y. Zhou, Z. P. Hu, Y. Li, J. Q. Xu, X. S. Tang, and Y. L. Tang, "$CsPbBr_3$ nanocrystal saturable absorber for mode-locking ytterbium fiber laser," Appl. Phys. Lett. **108**, 261108 (2016).
16. L. Protesescu, S. Yakunin, M. I. Bodnarchuk, F. Krieg, R. Caputo, C. H. Hendon, R. X. Yang, A. Walsh, and M. V. Kovalenko, "Nanocrystals of cesium lead halide perovskites ($CsPbX_3$, X = Cl, Br, and I): novel optoelectronic materials showing bright emission with wide color gamut," Nano Lett. **15**, 3692–3696 (2015).
17. Y. R. Yan, G. Chen, and P. G. Van Patten, "Ultrafast exciton dynamics in CdTe nanocrystals and core/shell CdTe/CdS nanocrystals," J. Phys. Chem. C **115**, 22717–22728 (2011).
18. Y. M. Zhao, C. Riemersma, F. Pietra, R. Koole, C. D. Donega, and A. Meijerink, "High-temperature luminescence quenching of colloidal quantum dots," ACS Nano **6**, 9058–9067 (2012).
19. J. Z. Li, S. F. Zhang, H. X. Dong, Y. F. Ma, B. Xu, J. Wang, Z. P. Cai, Z. H. Chen, and L. Zhang, "Ultrafast saturable absorption of core/shell colloidal quantum dots," Part. Part. Syst. Charact. **34**, 1600193 (2017).
20. J. Z. Li, H. X. Dong, S. F. Zhang, Y. F. Ma, J. Wang, and L. Zhang, "Colloidal quantum-dot-based silica gel glass: two-photon absorption, emission, and quenching mechanism," Nanoscale **8**, 16440–16448 (2016).
21. K. P. Wang, Y. Y. Feng, C. X. Chang, J. X. Zhan, C. W. Wang, Q. Z. Zhao, J. N. Coleman, L. Zhang, W. J. Blau, and J. Wang, "Broadband ultrafast nonlinear absorption and nonlinear refraction of layered molybdenum dichalcogenide semiconductors," Nanoscale **6**, 10530–10535 (2014).
22. S. B. Lu, L. L. Miao, Z. N. Guo, X. Qi, C. J. Zhao, H. Zhang, S. C. Wen, D. Y. Tang, and D. Y. Fan, "Broadband nonlinear optical response in multi-layer black phosphorus: an emerging infrared and mid-infrared optical material," Opt. Express **23**, 11183–11194 (2015).
23. S. B. Lu, C. J. Zhao, Y. H. Zou, S. Q. Chen, Y. Chen, Y. Li, H. Zhang, S. C. Wen, and D. Y. Tang, "Third order nonlinear optical property of Bi_2Se_3," Opt. Express **21**, 2072–2082 (2013).
24. B. Xu, S. Y. Luo, X. G. Yan, J. Z. Li, J. L. Lan, Z. Q. Luo, H. Y. Xu, Z. P. Cai, H. X. Dong, J. Wang, and L. Zhang, "CdTe/CdS quantum dots: effective saturable absorber for visible lasers," IEEE J. Sel. Top. Quantum Electron. **23**, 1900507 (2017).
25. G. J. Spuhler, R. Paschotta, R. Fluck, B. Braun, M. Moser, G. Zhang, E. Gini, and U. Keller, "Experimentally confirmed design guidelines for passively Q-switched microchip lasers using semiconductor saturable absorbers," J. Opt. Soc. Am. B **16**, 376–388 (1999).
26. M. B. Hisyam, M. F. Rusdi, A. A. Latiff, and S. W. Harun, "PMMA-doped CdSe quantum dots as saturable absorber in a Q-switched all-fiber laser," Chin. Opt. Lett **14**, 081404 (2016).
27. X. Zou, Y. Leng, Y. Li, Y. Feng, P. Zhang, Y. Hang, and J. Wang, "Passively Q-switched mode-locked Tm:LLF laser with a MoS_2 saturable absorber," Chin. Opt. Lett. **13**, 081405 (2015).